Near-Infrared Optical Absorption Behavior in High-β Nonlinear Optical Chromophore−Polymer Guest−Host Materials. 1. Continuum Dielectric Effects in Polycarbonate Hosts†

Richard R. Barto, Jr.*,‡ and Curtis W. Frank§

Departments of Materials Science and Engineering and of Chemical Engineering, Stanford University, Stanford, California 94304

Peter V. Bedworth, Susan Ermer, and Rebecca E. Taylor

Lockheed Martin Space Systems Company, Advanced Technology Center, Palo Alto, California 94304

Received: October 27, 2003; In Final Form: April 19, 2004

Optical waveguide technologies have been identified for broadband applications related to fiber network, airborne, and space-based communications. Active waveguide technologies developed around nonlinear optical (NLO) dye/polymer-based electrooptic devices have distinct advantages over existing RF communications in terms of cost, weight, size, bandwidth, and immunity to electromagnetic interference, but their ultimate applicability may be governed by optical loss. Though much attention has been given to the influences of the NLO chromophore optical nonlinearity, geometry, concentration, and poling effects on the bulk material nonlinearity and device performance, less attention has been directed at the effects of the component material properties and dye concentration on fundamental near-IR optical absorption. We investigate here the effects of polymer structural variations within the Bisphenol A polycarbonate family on near-IR absorption behavior of guest−host materials, holding the dye constant, over a range of dye concentrations. Solvatochromism plays an important role in the near-IR absorption loss of a particular NLO dye, (2-(3-cyano-4-{2-[5-(2-{4-[ethyl(2-methoxyethyl)amino]phenyl}vinyl)-3,4-diethylthiophen-2-yl]vinyl}-5,5-dimethyl-5*H*-furan-2-ylidene)-malononitrile). Near-IR loss vs dye absorption spectral shifts can be understood in terms of dye−polymer interaction energies within the context of Marcus' theory of polar contributions to initial and final electronic state free energies. The peak shift behavior can be described by the solvent polarity function of the polymer host, consistent with the Onsager continuum dielectric model. Analysis of the geometric parameters intrinsic to the generalized Kawski solvent polarity correlation suggests a more spherical dye shape can lead to reduced near-IR loss. The loss vs concentration results show that selection of a low-loss host polymer is a necessary but insufficient condition for establishing acceptable loss in a doped NLO dye−polymer system.

Introduction

The driving force for advances in photonic materials is the anticipated growth in data traffic for terrestrial, airborne, and space-based networks. Photonics technology has catalyzed enormous growth in the rate and efficiency of data transfer over long distances. Applications that involve point-to-point distribution of analogue signals have taken advantage of the superb signal carrying properties of optical fiber, through the use of RF-photonic links. Benefits of RF-photonic links for aircraft and space communications include the lightweight and small size of the optical fiber, their immunity to electromagnetic interference and electromagnetic pulses, low crosstalk, low on-board transmission loss, reduced power consumption, and greatly improved phase stability over a wide range of temperatures.[1]

RF-photonic links using external modulation minimize the undesirable effects seen in direct modulation of input laser current, such as chirp and poor linearity.[2] A Mach−Zender modulator (MZM) is an example of a commonly used external electrooptic (E-O) modulator, in which phase modulation is imposed on the optical carrier in one of two parallel waveguides by an incoming RF (signal) field, changing the refractive index of the active waveguide core material. Amplitude modulation is achieved through interference of the modulated light with that of the unmodulated, parallel waveguide. A phase change in the receiving arm of π radians yields complete destructive interference at the device output, corresponding to the device "half-wave" voltage, V_π.

A key figure of merit for an RF-photonic link is the available RF power gain g, which is proportional to $(\eta P/V_\pi)^2$, where η is the MZM optical efficiency and P is the optical input power to the MZM. The optical efficiency is inversely proportional to the total modulator fiber-to-fiber optical insertion loss T_{FF}. Thus, to optimize device performance, it is necessary to simultaneously minimize each of V_π and T_{FF} and maximize the modulator power handling capacity P. V_π is minimized by conferring high electrooptic activity, expressed by the electrooptic coefficient r_{33}, to the core MZM waveguide material.

Major advances in both r_{33} and device V_π have been achieved in recent years by using polymers containing nonlinear optical (NLO) chromophores possessing large microscopic first-order nonlinear susceptibility (or hyperpolarizability) β.[3] Organic NLO

† Part of the special issue "Alvin L. Kwiram Festschrift".
* Corresponding author. E-mail: Rick.barto@lmco.com.
‡ Department of Materials Science.
§ Department of Chemical Engineering.

10.1021/jp037239x CCC: $27.50
Published on Web 05/22/2004

materials have several advantages over $LiNbO_3$, including higher electrooptic activity, much lower dispersion from dc to optical frequencies, lower dielectric constant by an order of magnitude, and synthetic tailorability. The low device V_π provides development potential for much lower power operation, higher RF gain and lower noise figure than for $LiNbO_3$ devices, as well as for designs with multiple functions such as frequency conversion and generation. The lower dielectric constant and lower frequency dispersion characteristics offer the potential for much higher bandwidth operation, with polymer-based devices operating at the *W*-band (75−110 GHz) reported.[4]

Optimizing the r_{33} of these materials has been an area of intense theoretical and experimental research over the past decade.[5−19] A summary of materials synthesis and structural approaches to enhance r_{33} was given previously.[20] As discussed above, although high r_{33} (and low V_π) are of primary importance for achieving optimal link performance, several secondary parameters critically affect both link performance and device reliability. Recent work has been done to elucidate the potential for long-term thermal temporal stability of poling order of organic NLO guest−host materials.[21−24] Low fiber-to-fiber optical insertion loss T_{FF} is also crucial, which leads to stringent requirements on propagation loss in the E-O material. The ability to achieve high activity, high thermal-temporal stability, and low propagation loss concurrently in a single material has been hindered by a lack of understanding of mechanisms of optical loss in the near-IR.

This work attempts to address this limitation by systematically characterizing optical loss in these materials and developing structure−property relationships that will lead to a better understanding of optical loss mechanisms and strategies for minimizing loss without sacrificing nonlinear optical activity. We focus here on guest−host materials due to their process simplicity and reproducibility, some of which may find practical utility in prototype devices to meet proof-of-concept or interim technological development goals. The overall goal is to apply the lessons learned through this work to more complex material systems that should eventually aid in the development or more versatile, highly active, processible materials for large-scale device implementation.

To achieve higher E-O activity, the trend has been toward longer conjugation length and stronger acceptors, pushing the dye absorption maximum out to longer wavelengths, with spectral tails that can extend into the telecommunication wavelengths (1.3 and 1.55 μm). Absorption band shift behavior based on polymer host polarity is frequently observed, and line width variation has been associated with this solvatochromism.[25] Although the position, width, and shape of the dye absorption peak can influence the net optical loss in the near-IR, the influence of these spectral properties on near-IR absorption has not been investigated in detail. Moreover, the dye concentration dependence of near-IR loss is seldom reported.

We report here on a systematic study of the spectral properties of a high-β NLO dye, LMCO-4E6m (2-(3-cyano-4-{2-[5-(2-{4-[ethyl(2-methoxyethyl)amino]phenyl}vinyl)-3,4-diethylthiophen-2-yl]vinyl}-5,5-dimethyl-5*H*-furan-2-ylidene)malononitrile), incorporated as a guest in a series of Bisphenol A derivative polycarbonate homopolymers and copolymers, as a function of dye concentration. The dye is a direct structural analogue of LMCO-46m, with a diethyl rather than dihexyl pendant spacer group. LMCO-46m has been fully characterized in guest−host form with an amorphous polycarbonate copolymer, APC, for material properties and in experimental E-O devices, as reported previously.[21,26] The visible-to-near-IR spectrum of 4E6m doped in four polycarbonates over a range of concentrations (0−205 μmol/g polymer) was measured, and the concentration dependence of absorption loss at optical transmission wavelengths was determined. This absorption loss vs concentration dependence is compared to the energetic position and band shape of the dye $\pi-\pi^*$ electronic transition peak for each polymer host. We compare the solvatochromic behavior of the dye electronic transition and the near-IR loss−concentration dependence and consider thermodynamic and statistical models of inhomogeneous broadening and solvatochromism. The solvatochromic behavior for all four polycarbonates is described by a continuum dielectric model, which in turn is related to the near-IR loss behavior.

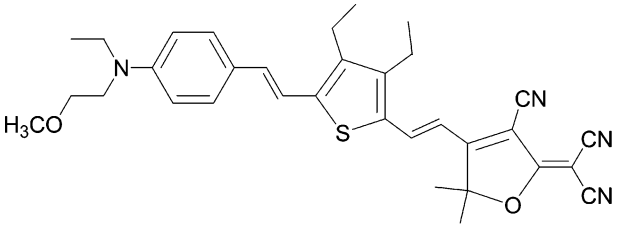

Figure 1. Nonlinear optical guest dye 4E6m: 2-(3-cyano-4-{2-[5-(2-{4-[ethyl(2-methoxyethyl)amino]phenyl}vinyl)-3,4-diethylthiophen-2-yl]vinyl}-5,5-dimethyl-5*H*-furan-2-ylidene)malononitrile.

To our knowledge, this is the first NLO polymer near-IR structure−property study to systematically investigate loss−concentration behavior and the relationships between near-IR loss and the main dye absorption peak.

Experimental Section

The structure of the NLO dye LMCO-4E6m used in all guest−host materials of this study is shown in Figure 1. This dye molecule is structurally analogous to the dye APTF-TC ("FTC," 2-(3-cyano-4-{2-[5-(2-{4-[bis(acetoethyl)amino]phenyl}-vinyl)-3,4-dibutylthiophen-2-yl]vinyl}-5,5-dimethyl-5*H*-furan-2-ylidene)malononitrile), which was developed by Dalton and co-workers[27] and is reported to have a large optical nonlinearity ($\mu\beta_0 = 14\,000 \times 10^{-48}$ esu at 1.9 μm). 4E6m is composed of three main components, an aminobenzene electron donor, a π-conjugated substituted thiophene ring bridge component, and an electron-accepting tricyanovinyldihydrofuran ring. It is synthesized by the Wittig reaction of {4-[(2-methoxyethyl)-ethylamino]benzyltriphenyl}phosphonium iodide with 3,4-diethylthiophene-2-carboxaldehyde to form a coupled product, which is then formylated to give the coupled aldehyde product. Reaction of the coupled aldehyde with 2-(dicynomethylene)-3-cyano-4,5,5-trimethyl-2,5-dihydrofuran (FTC acceptor) yields 4E6m.

Structures of the polymer hosts of this study are shown in Figure 2a−d. Each of these has Bisphenol A carbonate or a close analogue as a monomer unit. Two of these polymers are homopolymers, the experimental Red Cross polycarbonate (obtained from General Electric Global Research, $\bar{M}_w$ 49 000, Figure 2c) and Bisphenol A polycarbonate homopolymer (obtained from Scientific Polymer Products, cat. no. 035, $\bar{M}_w$ 43 000, Figure 2a). Note that though Red Cross is not strictly a Bisphenol A polycarbonate, it is a direct structural analogue of Bisphenol A. The remaining two polymers are random copolymers, the experimental copolymer poly[Bisphenol A carbonate]$_{0.25}$-*co*-[fluorenone carbonate]$_{0.75}$ (obtained from General Electric Global Research, $\bar{M}_w$ 35 000, Figure 2d) and "amorphous polycarbonate" poly[Bisphenol A carbonate]$_x$-*co*-[4,4′-(3,3,5-trimethylcyclohexylidene)diphenol carbonate]$_y$, where

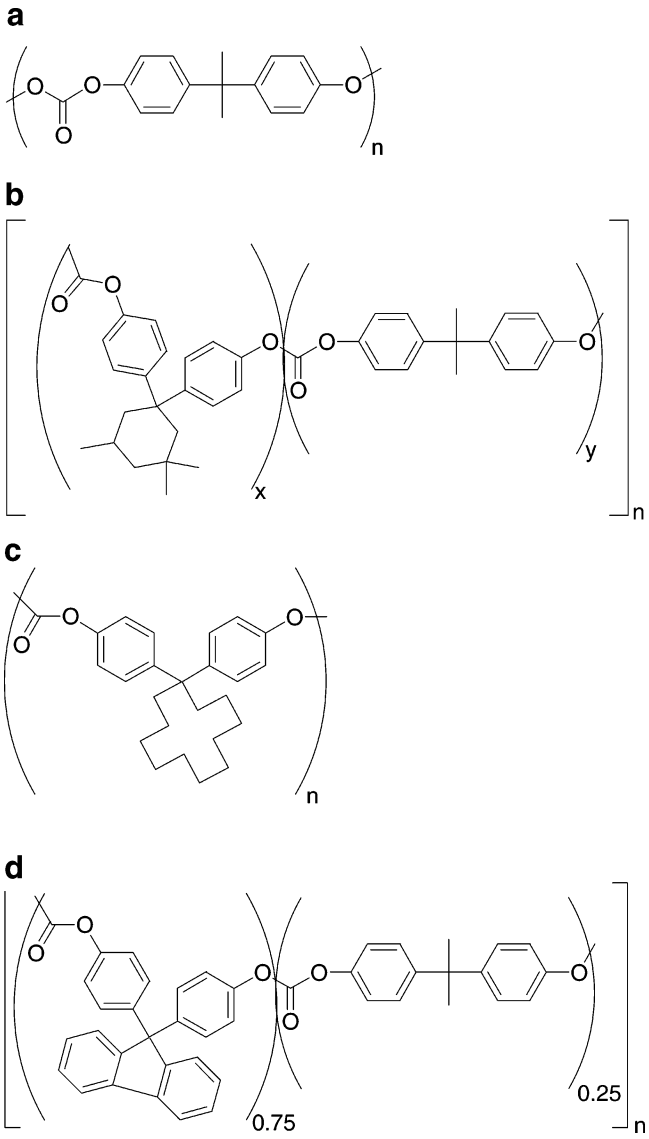

Figure 2. (a) Bisphenol A polycarbonate homopolymer. (b) Amorphous polycarbonate (APC): poly[Bisphenol A carbonate]$_x$-*co*-[4,4′-(3,3,5-trimethylcyclohexylidene)diphenol carbonate]$_y$, with $x \approx y$. (c) General Electric Red Cross polycarbonate. (d) General Electric Bisphenol A-*co*-fluorenone polycarbonate.

$x \sim y$ (APC, Aldrich cat. no. 43,057-9 $\bar{M}_w$ 69 000, Figure 2b). APC has been the subject of several studies of NLO guest−host materials with FTC-like chromophores.[20−22,26,28−33]

Each of the four polycarbonate hosts was doped with 4E6m at concentrations ranging from 0 to 205 μmol of dye/g of polymer, using 3:1 by weight mixtures of cyclopentanone and *N*-methyl-2-pyrrolidone, at polymer solids contents ranging from 5 to 15 wt %. The APC host was also doped at a higher 4E6m concentration of 330 μmol of dye/g of polymer. Film samples for spectral characterization were prepared on 1 in. diameter × 0.020 in. thick ultralow OH (<1 ppm) optical quality fused silica substrates. The substrates were precleaned using a Piranha (H_2SO_4:H_2O_2) process followed by a 10 s hydrofluoric acid dip. (**CAUTION!** Piranha is an aggressive and explosive chemical. Never mix piranha waste with solvents. Check the safety precautions before using it.) All samples were solution spin cast to yield final films of 1.7−6.6 μm in thickness, baked under nitrogen at a controlled ramp rate to 215 °C, held for 5 min, and cooled to <50 °C in less than 5 min. Film thickness was measured in at least two locations on each sample, using a Tencor Instruments Alpha-Step profilometer over small razor scratches. The films were examined visually and at 50−200× and judged to be of acceptable quality for spectral characterization if they exhibited thickness and color uniformity and lacked crystals or distinct phases.

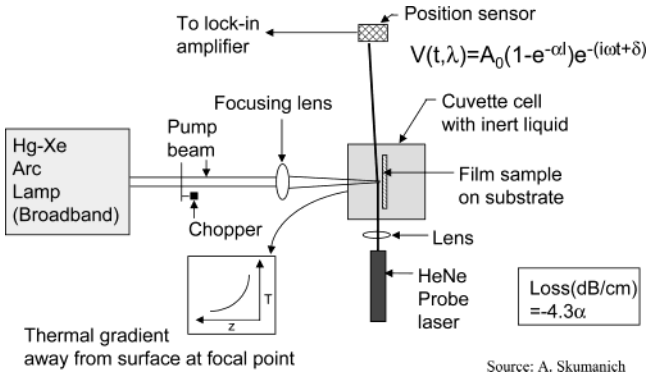

Figure 3. Schematic representation of photothermal deflection spectroscopy operation principles.

The vibrational overtones lying in the near-IR region arise from the anharmonicity of fundamental modes, such as C−H, O−H, or N−H stretches. The mode anharmonicity increases the probability of observing a forbidden $\Delta v > 1$ state, due to a deviation from a quadratic Morse potential. The positions of these overtones provide the physical basis for the choice of optical transmission frequencies. These overtones are extremely weak relative to electronic transitions and are not detected by conventional reflectance and transmission techniques. Sensitive photothermal spectroscopy techniques, such as thermal lensing, photoacoustic spectroscopy (PAS) or photothermal deflection spectroscopy (PDS) can resolve these transitions, as well as the presence of weak tail states of comparable magnitude from the dye main absorption peak. A well-accepted approach for characterizing the continuous spectrum from the high energy dye electronic transition peak in the visible region to the weak absorption in the near-IR region, is to use a combination of UV−vis transmission spectroscopy and PDS. Among the photothermal methods, PDS appears to exhibit the greatest sensitivity for absorption measurements of condensed phases at room temperature.[34] The pioneering work on PDS was conducted by Jackson and Amer,[35] which showed that PDS senses, to a high level of fidelity, optical attenuation nearly completely due to absorption by the material (as opposed to scattering, reflection, and refraction).

The principles of PDS are shown schematically in Figure 3, and the PDS experimental configuration is shown in Figure 4. PDS uses chopped radiation at low frequency (<30 Hz) to illuminate a solid film sample suspended in a transparent, thermally conductive inert liquid. During an "on" chopping cycle at a given wavelength, the absorbed radiation excites electronic or vibrational states of the species present in the illuminated region. During the "off" cycle, the heat produced by nonradiative relaxations thermally diffuses out of the sample. If the sample thickness is much less than the thermal diffusion length of the film material (as is the case for the subject films), the heat emitted from the film, and hence the optical absorption, is characteristic of the bulk material.[36] The emitted heat induces a thermal gradient in the liquid near the sample surface that gives rise to a refractive index gradient. An optical probe beam directed through the fluid adjacent and parallel to the heated sample surface experiences an angular deflection away from the sample as a result of the index gradient. Probe beam deflection resolution of <1 nm has been reported for commercially available position sensing photodiode detectors,[37] for

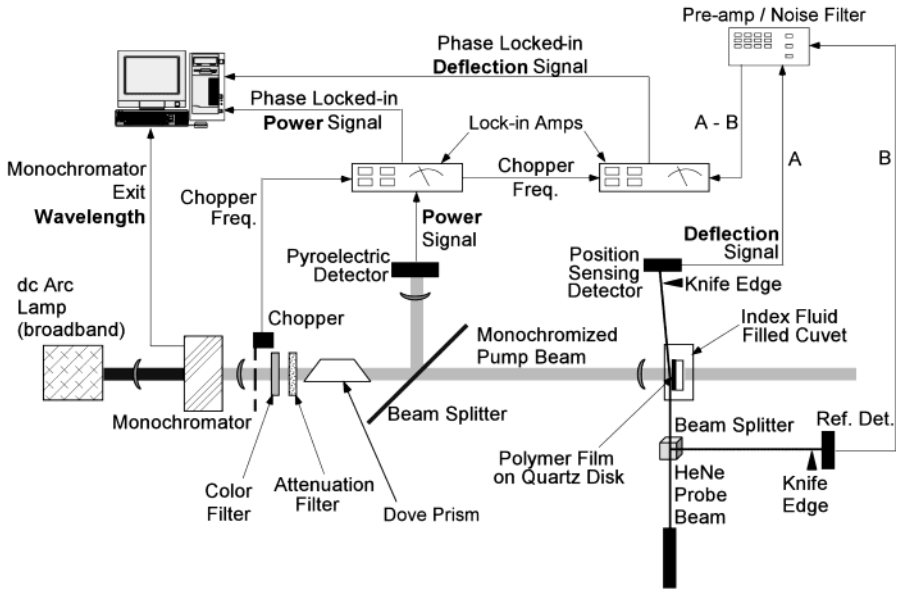

Figure 4. Schematic of PDS experimental configuration.

temperature changes as little as 10^{-8} °C in liquids.[36] Optical propagation and thermal analyses by Rosencwaig[38] and others have shown that the probe beam angular deflection can be directly related to the temperature gradient in the fluid, which in turn can be related to the optical absorbance.[38,39] For optically thin samples, these relationships reduce to a simple expression for the ac deflection signal V_{ac} in terms of α, the optical absorption coefficient at a given wavelength λ:

$$V_{ac}(\lambda) = I_0(\lambda)(1 - R)(1 - e^{-\alpha(\lambda)l})S \quad (1)$$

where $\alpha(\lambda)$ is the optical absorption coefficient at wavelength λ, I_0 (λ) is the optical input power at wavelength λ, R is the reflection coefficient of the sample, S is a lumped factor due to the thermal properties of fluid and substrate, and l is the sample film thickness.

A highly absorbing, optically flat blackbody, used as a calibration standard, has a deflection signal expressed analogously as

$$V_{ac}^{std}(\lambda) = I_0(\lambda)(1 - R^{std})(1 - e^{-\alpha(\lambda)l})S \quad (2)$$

It follows that the absorption coefficient at a given wavelength can be expressed in terms of the ac deflection signal by

$$\alpha(\lambda) = -\frac{1}{l}\ln\left(1 - \frac{\bar{X}_{pds}}{1 - R}\right) = -\frac{1}{l}\ln\left(1 - \frac{\bar{X}_{pds}}{\bar{X}_{sat}}\right) \quad (3)$$

where $\bar{X}_{pds}$ is the blackbody standard-normalized PDS signal, given by

$$\bar{X}_{pds} = V_{ac}/V_{ac}^{std} \cong (1 - R)(1 - e^{-\alpha(\lambda)l}) \quad (4)$$

and $\bar{X}_{sat}$ is the normalized PDS signal at thermal saturation in the limit of strong absorption.

The PDS test bed used a 1 KW Hg(Xe) dc short arc lamp as the broadband illumination source at 12.6 Hz chopping frequency, with a $^1/_8$ m dual-grating monochromator. The source beam image is a vertical ellipse, which is focused through vertical entrance slits to the monochromator at a divergence nearly matching that of the monochromator (*f*/3.7). To increase the length of interaction between the sample illuminated region and the probe beam, and thereby improve signal-to-noise, a Dove prism was used in the beam path (see Figure 4) to rotate the beam image by 90°, rendering it horizontal when focused onto the sample. A portion of the pump beam was split off and focused onto a pyroelectric detector to monitor optical power input at each wavelength via a lock-in amplifier. The probe beam was a 10 mW CW HeNe laser, attenuated to ∼1.5 mW. The sample disk was mounted inside a special fixture composed of a back plate that slightly bends the vertical centerline of the sample into the probe beam. The fixtured sample was held inside a fused silica cuvette and filled with 3M Fluorinert Liquid FC-72 as the index fluid. The cuvette was closed with an O-ring sealed lid to prevent fluid evaporation. The cuvette was placed in a custom holder on a rotational translation stage attached to a triple axis translation stage, permitting precise alignment of the sample surface to the probe beam for maximized signal. Probe beam deflection was detected using a pn photodiode with an op-amp drive circuit providing gain and zero offset control. A blackened razor was used in front of the detector to shadow half of the probe beam. The probe beam was 50−50 split to a replicate reference detector prior to the sample. The primary and reference detector dc signals were conditioned with a preamplifier, with the difference signal forwarded to a second lock-in amplifier. This scheme provided cancellation of probe beam pointing noise.

PDS scans were performed by measuring deflection signal, input power, and phase lag at each wavelength, scanning from low energy to high energy in 10 nm increments. Low energy scans were performed first from 1830 to a minimum of 870 nm to reduce the possibility of photobleaching near the absorption maximum. A second, high energy scan was performed from 1830 to 600 nm for the dual purpose of finding the PDS saturated signal (strong absorption limit) and checking for any photobleaching effects from previous scans. A UV−vis absorption spectrum was collected in transmission mode on the same sample using a Cary 5E spectrophotometer, scanning from 1100 to 300 nm, to complete the optical absorption spectrum through the regions of overlap between PDS and Cary transmission data and the absorption maximum.

Results

Representative PDS−Cary spectral comparisons of a concentration series of 4E6m guest−host mixtures are shown in

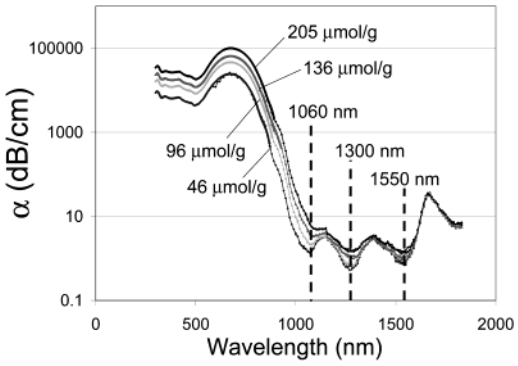

Figure 5. Typical concentration series of photothermal deflection spectroscopy absorption loss spectra for 4E6m/polymer guest−host materials. Shown are data for 4E6m/polycarbonate homopolymer.

Figure 5, for the case of 4E6m/polycarbonate homopolymer. For each series, the spectra are composed principally of four peaks: (1) a strong main electronic absorption peak of the dye in the visible region, λ_{max} 664−681 nm; (2) a $\nu_{0,3}$ C−H stretching doublet centered at ∼1170 nm; (3) a $|2,1\rangle$ C−H stretching-plus-bending combination overtone at 1390 nm; (4) a $\nu_{0,2}$ C−H stretching overtone at 1660 nm.[40] For each 4E6m/polymer concentration series, the main peak shows a general progression with concentration, as expected according to the Beer−Lambert law, with approximately Gaussian peak shape when plotted on an energy scale. The absorption maximum was well resolved for samples except for those at the highest concentration. Note that the strengths of the $|2,1\rangle$ C−H overtone peak at 1390 nm and the $\nu_{0,2}$ C−H overtone at 1660 nm do not appear to be sensitive to dye concentration, indicating very similar concentrations of C−H moieties between doped and undoped polymers. Excellent spectral repeatability was observed in most cases.

Of primary interest are the values of losses at the telecommunication transmission wavelengths, between the overtone peaks. A general progression of absorption loss versus concentration is observed for each 4E6m/polymer concentration series at these wavelengths. In the analysis of polymer host effects on absorption loss behavior, three key aspects of the spectra were examined: (1) the concentration dependence of loss at the minima between overtone peaks (at 1060, 1300, and 1550 nm); (2) the broadening behavior of the dye electronic absorption peak; (3) the energetic shifting behavior of the dye absorption maximum. The concentration dependence of absorption loss minima is plotted in Figure 6a−c for 4E6m in all four polymers at each wavelength. Approximately linear behavior of the absorption minima with concentration is exhibited for 4E6m doping of each polymer host, with the best correlation at 1060 nm (R^2 range 0.97−0.98), followed by 1300 nm (R^2 range 0.90−0.94), and finally by 1550 nm (R^2 range 0.10−0.96). The poor correlation for 4E6m/Red Cross at 1550 nm is attributed to nearly zero concentration dependence of loss at 1550 nm for this system.

The slope of the PDS loss minimum versus concentration plot is treated as a characteristic material property for each 4E6m-polymer guest−host combination, analogous to a molar absorptivity, at each wavelength minimum. The intercept values for loss vs concentration at 1060 nm are in reasonable agreement between polymers and are relatively low compared to doped polymer loss values. The loss−concentration behavior at 1060 nm is consistent with the Beer−Lambert law, dominated by dye electronic absorption peak broadening with increased concentration. Moreover, variation in loss between polymers at near-zero concentration is relatively small compared to variation in loss−concentration dependence. This is due to the proximity of 1060 nm absorption minima to the strong absorption region of the dye spectrum, where changes in absorption due to dye concentration and peak position are more important to loss than the contribution of polymer structural variation.

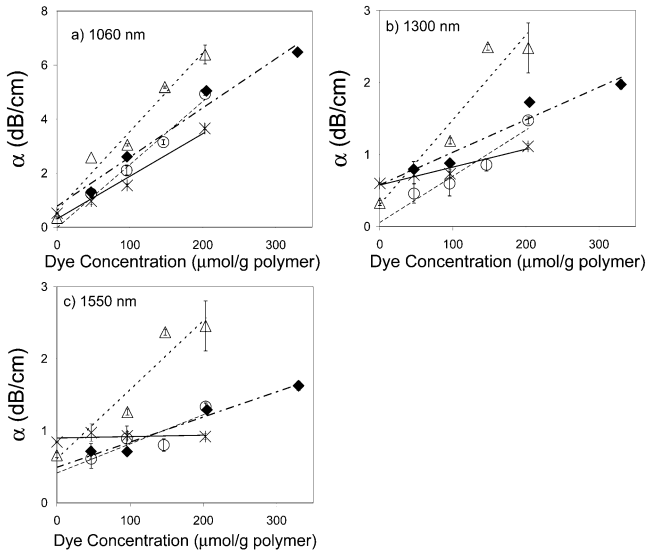

Figure 6. Measured PDS absorption loss vs dye concentration for 4E6m/Bisphenol A polycarbonate homopolymer and copolymer guest−host materials at (a) 1060 nm, (b) 1300 nm, and (c) 1550 nm. Polymer hosts denoted by * for Red Cross polycarbonate, ◆ for APC, ○ for polycarbonate homopolymer, and △ for Bisphenol A-*co*-fluorenone polycarbonate.

Variations in near-zero loss values with polymer structure at 1300 and 1550 nm are similar to those at 1060 nm, but are more significant relative to changes with dye concentration because this is the far red tail of the main dye absorption peak. This is not unexpected, because it is well established that there can be considerable variation in the near-IR absorption spectrum of neat (undoped) polymers.[23,41−43] Of chief consideration for this study is the variation in absorption with dye concentration above the values for undoped polymers, which is felt to represent the unique dependence of the main peak broadening or shifting behavior on polymer structure. The absorption loss−concentration slope was taken to be a fundamental material property associated with the dye−polymer structure pair and used in the evaluation of structure−property relationships. Moreover, it is seen from the near-zero concentration loss values that choice of a low-loss neat polymer, though necessary for yielding low loss in a doped system, is not adequate for achieving low loss at the higher dye loading levels needed to achieve the highest possible nonlinearity for a given dye in a given host. The influence of polymer environment is a more important determinant of loss at higher dye concentrations.

Discussion

The combination of UV−vis with PDS near-IR absorption spectra provides detailed information spanning part of the peak associated with the polymer $\pi \rightarrow n^*$ intramolecular transition, the complete dye $\pi \rightarrow \pi^*$ electronic transition peak, vibronic states covering both dye and polymer and any coupling between them, and overtones of proton stretch and bend vibrations. Owing to the broad nature of the $\pi \rightarrow \pi^*$ transition in amorphous glasses, the low energy side of the dye electronic absorption peak can convolve the specific features associated with other processes, completely dominating vibronic features in the visible-to-near-IR, and contributing significantly to the

strength of forbidden transitions in the near-IR. The dye absorption peak shape and energy position are very sensitive to the molecular environment and microstructure, and therefore, the influence of the dye absorption peak in the near-IR region was of primary interest for this study.

Stegeman and co-workers[44] conducted a study of the effect of chromophore structure and polymer environment on the log slope of the infrared tail of the absorption peak by treating the optical spectrum (on a wavelength scale) as a Voight profile. Agreement was shown between predicted absorption loss by extrapolation of the log-linear Voight slope to 775 nm and planar waveguide propagation loss measurements at 775 nm, for azo dye guests in a PMMA host for absorption losses of at least 1 db/cm. A correlation was found between the log-linear Voight profile slope and glass transition temperature (T_g) for azo guest dyes in six different polymer hosts, in which higher projected loss at 775 nm was found for increasing polymer host T_g. However, no meaningful correlations were observed between either calorimetric host polymer T_g values or PDS-measured loss at 1060, 1300, and 1550 nm of the present study and Voight profile slope, and thus, the Voight profile fitting approach was abandoned. As described in the following sections, a more detailed analysis of the dye absorption peak was adopted to more precisely describe the polymer structural attributes responsible for absorption loss behavior.

Inhomogeneous Broadening and Solvatochromism. The dye main absorption peak width and shifting behavior of each of the 4E6m-doped polymer systems was carefully examined in the context of inhomogeneous broadening and solvatochromism. For liquids and glassy amorphous solids, the peak width is typically hundreds of cm^{-1}, which is considerably broader than those of crystals ($\sim$1 cm^{-1}).[45] The spectral broadening is brought about by statistical fluctuations of surrounding solvent molecules[45,46] and chromophore conformations.[47] These local fluctuations give rise to a distribution of electronic energy gaps and an ensemble-averaged spectrum that is inhomogeneously broadened, as reflected in the standard deviation about the peak absorption frequency. For dye/polymer systems, the configurational relaxation in the excited state is well described by an inhomogeneous broadening model in which the dye molecules in a glassy solid polymer solution are treated as an ensemble of centers of $\pi \rightarrow \pi^*$ transitions of varying frequencies.[46] Kjaer and Ulstrup[48] showed that a single Franck−Condon envelope of Gaussian subpeaks can be convolved to reproduce the asymmetric, broad, solvatochromic absorption peak of merocyanine dyes for a wide range of aprotic solvents.

Theoretical analyses of optical absorption band shapes of solute−solvent systems have been extensively reported for both liquid and condensed phase systems.[45−55] Kador[49] derived an exact form of the inhomogeneously broadened band shape for an ensemble of chromophores in a disordered solid matrix by following a stochastic theory based on Markoff statistics. The inhomogeneous band shape was found to be

$$I_G(\nu) = (2\pi\sigma_s)^{-1/2} \exp\left(\frac{-(\nu - \nu_s)^2}{2\sigma_s^2}\right) \tag{5}$$

where ν_s, the "solvent shift", is the displacement of ν_{max} from the vacuum absorption frequency, and σ_s is related to the inhomogeneous peak width (full-width at half-max FWHM) through

$$\sigma_s = \Gamma_s/2\sqrt{2\ln 2} \qquad \Gamma_s = \text{FWHM} \tag{6}$$

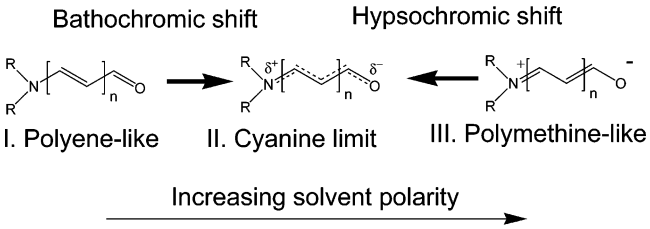

Figure 7. Polyene-to-zwitterion merocyanine solvent polarity scale.

This form of the inhomogeneous band shape is seen to be Gaussian. Obato, Machida, and Horie[56] followed Kador's analysis to show that the broadening term can be related to van der Waals (W) and dipole−dipole (D) interaction terms for a polar dye molecule in a nonpolar or weakly polar polymer, through

$$\Gamma_s = \sqrt{\frac{32\pi \ln 2}{9}\rho R_c^3 (W^2 + D^2)} \tag{7}$$

with

$$W = 4\epsilon_U\left(\frac{\sigma}{R_c}\right)^6 \tag{7a}$$

$$D = \frac{2\Delta\mu\mu_M}{4\pi\epsilon_0 hcR_c^3} \tag{7b}$$

where σ is the matrix molecule radius, R_c is the solute cavity radius, $\Delta\mu$ is the difference between solute excited and ground state dipole moments, μ_M is the matrix dipole moment, ϵ_U is the depth of the interaction potential well, ϵ_0 is the permittivity of free space, h is the Planck constant, and c is the speed of light in a vacuum.

Equation 7 indicates that both van der Waals and dipole−dipole interactions contribute to Γ_s. This expression will be shown later to be useful for relating experimentally observed inhomogeneous broadening to the dye−polymer interactions, expressed in terms of the component solubility parameters.

The solvatochromic behavior of the merocyanine class of dyes in solvents has been well documented.[14,18,19,57−63] Reichardt and Dimroth[57] developed the well-known $E_T(30)$ scale for solvent polarity, which describes the ground-to-excited state transition energy shift relative to pyridinium *N*-phenoxide betaine dye ("dye #30") for a wide range of solvents. Because the excited state of high-β chromophores has significant intramolecular charge-transfer nature, the chromophore electronic structure is strongly solvent polarity dependent. The magnitude of $E_T(30)$ has been related to changes in the electronic structure and dipole moment on electronic transition for dyes that are more dipolar in the excited state than in the ground state and can be directly related to the dielectric properties of the solvent medium.

In the bond-length alternation (BLA) theory of Marder and co-workers,[18] the linear and nonlinear optical properties of chromophores are related to their structure through the degree of bond-length alternation (BLA), defined as the average difference between single and double bond lengths along the π-conjugated bridge, due to distortion from the equilibrium configuration by substituent and/or solvation effects. A merocyanine dye may take on a range of mesomeric structures of varying degrees of Zwitterionic character depending on the dye structure and the strength of either an applied external field or an effective internal field associated with the polarity of the surrounding matrix. This effect is depicted in Figure 7. The

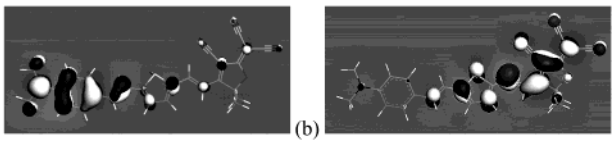

Figure 8. Accelrys, Inc. Materials Studio DMOL3 simulations of LMCO 46 molecule HOMO (a) and LUMO (b), illustrating charge transfer between the two states.

polymethine (charge-separated) structure (III), of higher BLA, is more energetically stable for solvent-mediated polarization; i.e., a more polar solvent stabilizes charge separation. A ground state structure of 4E6m falling closer to polyene (I) on the bond-length alternation scale is expected to display a shift toward the mixed equilibribrium cyanine state (II) as polymer polarity increases and decrease the transition energy toward longer wavelengths, i.e., a "red shift." This behavior is defined as bathochromism, whereas the opposing behavior is referred to as hypsochromism. This interaction leads to an effective internal field acting across the π-conjugated bridge that influences both the ground state structure and the response of the structure to a small perturbing field, i.e., the polarizabilities α, β, and γ of orders 1, 2, and 3, respectively.

The second-order polarizability β can be determined from

$$\beta_{xxx}(-2\omega;\omega,\omega) = \frac{e^3|\mu_{eg}|^2(\mu_e - \mu_g)}{\hbar^2} \frac{3\omega_0^2}{(\omega_0^2 - \omega^2)(\omega_0^2 - 4\omega^2)} \tag{8}$$

where μ_e and μ_g are the permanent excited and ground state dipole moments, respectively, μ_{eg} is the transition dipole moment between the two states, ω is the optical frequency, ω_0 is the peak transition frequency, e is the electron charge, and $\hbar$ is the Planck constant.[64] This expression shows that a strong solvent shift may be accompanied by a change in hyperpolarizability (nonlinear activity), depending on the position of the chromophore along the bond-length alternation scale.

An extension of these analyses was conducted by Marks and co-workers,[14] in which a self-consistent reaction field model[14,65] was used to account for the solvent polarity-driven internal field for merocyanine chromophores. In the Onsager continuum dielectric model, the dye solute comprises a spherical cavity bathed by a continuum matrix of a given dielectric constant. The surrounding medium is polarized by the permanent dipole moment μ_g of the dye, inducing a so-called self-consistent reaction field (SCRF) in the polarized matrix that in turn acts back on the solute to stabilize charge separation in the ground and excited states. Predicted values of transition energies vs SCRF showed bathochromism, with a change to hypsochromism at higher SCRF for a dye exhibiting aromatic stabilization upon charge separation. Calculated SCRFs were large enough to drive each NLO property through maxima and minima to slightly beyond the cyanine limit, showing that increasing the solvent polarity can improve the nonlinear optical activity (β) up to a point, but physically solvent accessible polarities may be reached such that β is degraded or even driven to near-zero values.

We have modeled the distribution of π-electron charge density in the ground and excited states for a 4E6m analogue containing no pendant dialkyl spacer groups by an ab initio density functional theory calculation using DMOL3 from Accelrys, Inc. The results are displayed graphically in Figure 8, showing more polyene-like (I) character in the ground state and more zwitterionic character in the excited state. For a dipolar solute surrounded by a nonpolar solvent, the transition energy is largely influenced by dipole−induced dipole and dispersion forces, and the Franck−Condon excited state is more readily solvated by dipole−solvent polarization.

In the seminal treatment by Marcus,[66] the thermodynamic average energy difference between ground and excited states was estimated by accounting for permanent dipole−induced dipole moments for the polar part of the interactions, and contributions of dispersions and polar interactions to the spectral shift were found to be additive. Within this theoretical framework, Marcus showed that the peak transition frequency is the free energy difference between ground and excited states combined with the solvent reorganization energy E_s (associated with the Gibbs free energy of solvation), related to the inhomogeneous broadening width σ_s in eq 5 as

$$\sigma_s = \sqrt{2E_s kT} \tag{9}$$

The relationship between the broadening σ_s and peak shift $\Delta\nu_{max}$ ($=\nu_s$, eq 5) can be expressed as

$$\sigma_s^2 = A_0\Delta\nu_{max} + B_0 \tag{10a}$$

or

$$\Gamma_s^2 = A\Delta\nu_{max} + B \tag{10b}$$

where A's and B's are constants.

Expanding on Marcus' treatment, Matyushov and Schmid[61] showed that the chemical potential of solvation can be described as first and second-order energy shifts, where a solvatochromic shift is a first-order shift, and inhomogeneous broadening is a second-order shift. Sevian and Skinner[63] have shown through a perturbative analysis of transition energies that a large inhomogeneous width compared to size of a red shift is due to large density fluctuations.

The solvent reorganization energy is expressed in the classic continuum approximation as

$$E_{sc} = \frac{\Delta\mu^2}{R_0^3}\left(\frac{\epsilon - 1}{2\epsilon + 1} - \frac{n^2 - 1}{2n^2 + 1}\right) \tag{11}$$

where n and ϵ are the solvent refractive index and dielectric constant, respectively. This is consistent with experimentally observed correlation of solvatochromic shifts of ν_{max} in nonpolar fluids with functions of n^2 and ϵ, interpreted in the Onsager reaction field model as the influence of solute−solvent dispersion interactions, which are stronger contributors as solvent polarity increases.

Experimental fwhm vs ν_{max}. The UV−vis $\pi \rightarrow \pi^*$ transition peak for 4E6m doping at the highest common dye concentration studied, 205 μmol dye/g of polymer (10.1 wt %), is represented as overlay spectra for the Bisphenol A polycarbonate host polymer series in Figure 9 showing mild solvatochromic shifting behavior. To examine the inhomogeneous broadening and solvatochromic behavior, Gaussian peak fits were carried out on each of the UV−vis spectra, and the parameters of full-width at half-maximum (FWHM $= \Gamma_s$) and ν_{max} were derived from the equation of the fit to Figure 5. To test for adherence of the broadening and solvent shift behavior to the Marcus model, Γ_s^2 was plotted against ν_{max}, as shown in Figure 10. The data are well correlated for 4E6m doping for all polymer hosts studied, indicating qualitative agreement with the Marcus model (eq 10b). This treatment depends on the dielectric properties of the polymer (real and imaginary parts of the dielectric constant, described by n^2 and ϵ, respectively) and

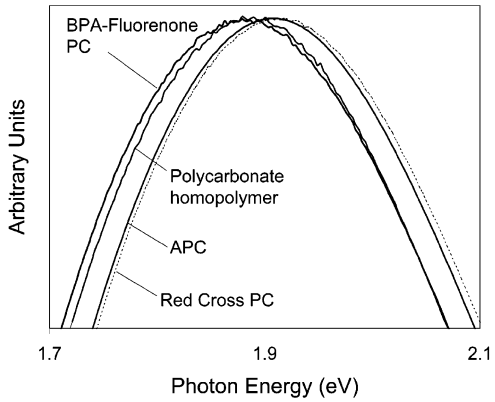

Figure 9. UV−vis absorption spectra for series of 4E6m/Bisphenol A polycarbonate series of guest−host materials at dye concentration of 205 μmol/g of polymer (10.1 wt %).

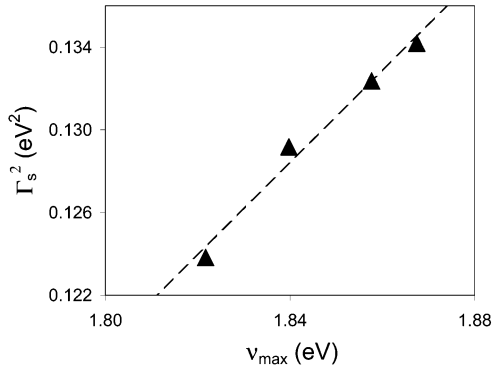

Figure 10. Square-inhomogeneous width (Γ_s^2) vs main peak position (ν_{max}) for 4E6m/Bisphenol A polycarbonate series of guest−host materials at a dye concentration of 205 μmol/g of polymer (10.1 wt %).

suggests that solvatochromism and inhomogeneous broadening of 4E6m doped polycarbonates follow classical Onsager dielectric continuum behavior, such that the solvent shift can be assigned to a solvent reorganization energy E_{sc}.

The dielectric continuum behavior is described by the solvent polarity, the spherical radius of a virtual cavity occupied by the dye, and the dipolar parameters of the dye (ground and excited state dipole moments and polarizability), with additive contributions by dispersion forces and polar interactions. As discussed above, a more polar polymer medium is expected to impart a greater solvent shift. The analysis of Sevian and Skinner[63] suggests that the less shifted, more broadened dye−polycarbonate spectra are due to greater density fluctuations, which could arise from a less uniform distribution of dye molecules in the polymer host, due to poorer solubility. Note that this behavior is also predicted by application of the coherent potential approximation on Drude particles in a cermet topology[53] and will be shown to be consistent with predicted dye and polymer solubilities later in the discussion.

Although variations in the dye structure were not investigated, the agreement of the first- and second-order shift behavior with Marcus theory suggests that greater broadening and weaker solvatochromism should occur as the dye molecular size decreases, which is in agreement with the results of an analysis of solvent shifts vs a generalized solvent polarity function discussed later. The solvatochromic behavior in this polycarbonate series implies a tradeoff may exist between the near-IR loss behavior and the hyperpolarizability of the doped polymer system, provided a relationship exists between near-IR absorption and the main absorption peak.

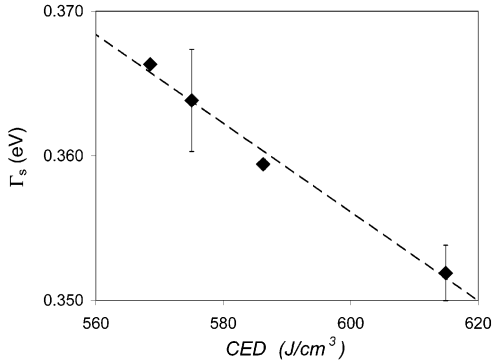

Figure 11. Inhomogeneous absorption peak width (Γ_s) vs cohesive energy density (CED) determined from geometric mean Fedors-calculated dye−polymer solubility parameter ($\delta_{dye}\delta_{polymer}$) for 4E6m/Bisphenol A polycarbonate series of guest−host materials at a dye concentration of 205 μmol/g of polymer.

Relationships between fwhm and Solubility Parameter δ. The relationship between the inhomogeneous width Γ_s and density fluctuations in the Bisphenol A polycarbonate family of 4E6m doped guest−host systems of this study was examined more quantitatively by considering the potential energy of dye−matrix attractive interactions. This can be expressed by the cohesive energy density CED,[67] defined in terms of the molar interaction energy ΔE_v (the free energy of vaporization) and the molar volume V_m as

$$\mathrm{CED} = \Delta E_v/V_m = (\Delta H_v - RT)/V_m \qquad (12)$$

By definition,[67] the solubility parameter δ is

$$\delta = \sqrt{\mathrm{CED}} \qquad (13)$$

In the solution theories of Hildebrand and Scott[68] and Scatchard,[69] the geometric mean of the dye and polymer CED is used to approximate the dye−matrix intermolecular potential

$$\mathrm{CED}_{dp} \cong \sqrt{\delta_{dye}{}^2\delta_{polymer}{}^2} = \delta_{dye}\delta_{polymer} \qquad (14)$$

The above expression suggests that the interaction forms after dissociation of dye−dye and polymer−polymer interactions. From the expression for Γ due to Obato, Machida, and Horie (OMH)[56] (eq 7), given in terms of van der Waals (W) and dipole−dipole (D) components, a linear relationship between Γ_s and $\delta_{dye}\delta_{polymer}$ is expected. With the dye and polymer solubility parameters δ_{dye} and $\delta_{polymer}$ calculated following the group contribution model given by Fedors,[70] a strong linear correlation ($R^2 = 0.99$) is displayed between Γ_s and $\delta_{dye}\delta_{polymer}$ as shown in Figure 11. Such behavior is in accordance with the OMH model and is consistent with Kador's stochastic lattice irregularity theory based on dipole−dipole and van der Waals interactions. This behavior qualitatively shows that as the dye−matrix attractive interaction strength diminishes, as reflected in smaller values of the polymer solubility parameter, broadening is enhanced due to less compositional uniformity, and possibly some degree of dye aggregation, resulting in dipole density fluctuations in the matrix.

Relationships between ν_{max} and Solubility Parameter δ. To quantitatively explore the effect of density fluctuations in 4E6m doped polycarbonates on the frequency position of the peak transition ν_{max}, governed by polymer-specific solvatochromic shifts, the dye−polymer enthalpy of mixing, based on regular solution theory, was considered. The Hildebrand and

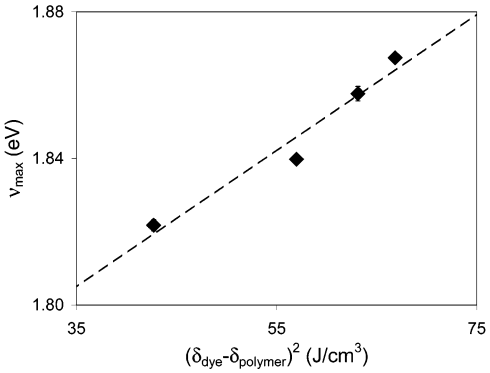

Figure 12. Main peak position (ν_{max}) vs Fedors-calculated solubility parameter difference for 4E6m/Bisphenol A polycarbonate series of guest−host materials at a dye concentration of 205 μmol/g of polymer.

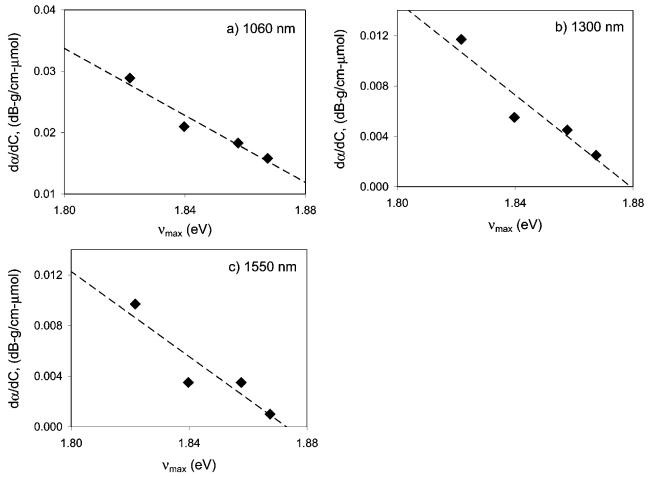

Figure 13. Measured PDS absorption loss−concentration slope vs main absorption peak position for 4E6m/Bisphenol A polycarbonate series of guest−host materials at a dye concentration of 205 μmol per gram of polymer (10.1 wt %), at wavelengths (a) 1060 nm, (b) 1300 nm, and (c) 1550 nm.

Scott relation for the heat of mixing ΔH_M[71] for a dye−polymer mixture is

$$\Delta H_M = V_M(\delta_{dye} - \delta_{polymer})^2 \upsilon_{dye}\upsilon_{polymer} \qquad (15)$$

where V_M, υ_{dye}, and $\upsilon_{polymer}$ are the total mixture volume and volume fractions of dye and polymer, respectively. Here it is assumed that the volume fractions of dye and polymer are constant among the various polymer hosts for the reference dye concentration of 205 μmol/g of polymer, so for a given volume element, the heat of mixing is proportional to $(\delta_{dye} - \delta_{polymer})^2$. Larger values of ΔH_M correspond to poorer solubility, so according to the results of the analysis by Sevian and Skinner, smaller solvent shifts, and hence larger values of ν_{max}, are expected for greater solubility parameter differences.

Using the previously calculated values of δ_{dye} and $\delta_{polymer}$ by the Fedors model,[70] a plot of ν_{max} vs $(\delta_{dye} - \delta_{polymer})^2$, shown in Figure 12, does indeed give a relatively strong linear correlation ($R^2 = 0.96$) for the 4E6m doped polycarbonate family and is consistent with Marcus $\Gamma_s^2 - \nu_{max}$ behavior, because the distribution of dipole−dipole interactions is expected to become less uniform with decreased dye solubility. The observed $\nu_{max} - (\delta_{dye} - \delta_{polymer})^2$ correlation would also be in line with greater solvent shifts (lower ν_{max}) at higher polymer polarities, because the dye solubility very likely improves ($(\delta_{dye} - \delta_{polymer})^2$ decreases) with increased solvent polarity. This proposition is examined later in the discussion.

The results of both the experimental Γ_s and ν_{max} variation with dye−polymer solubility show that to a reasonable degree, the peak shifting and inhomogeneous broadening behavior of 4E6m doped polycarbonate can be predicted by calculated values of dye and polymer solubilities. For the doped polycarbonate series, the Fedors group contribution model is shown to be a reliable predictor of these trends. The ability to understand and predict the solvent shifting behavior in the 4E6m/polycarbonate series will be shown to be important to understanding the near-IR loss behavior in the next section.

Experimental Loss−Concentration Slope dα/d*C* vs ν_{max}. The main absorption peak width Γ_s and peak frequency ν_{max} for each dye−polymer pair were correlated with the experimentally determined absorption loss vs concentration slopes (dα/d*C*) at each of 1060, 1300, and 1550 nm, and displayed for the dα/d*C*−ν_{max} data in Figure 13a−c. Linear correlations are seen for dα/d*C* vs ν_{max} at 1060 nm ($R^2 = 0.995$), 1300 nm ($R^2 = 0.90$), and 1550 nm ($R^2 = 0.85$), with dα/d*C* decreasing with increasing ν_{max} (decreasing solvent shift). This loss−ν_{max} behavior implies a near-IR absorption loss mechanism largely controlled by solvatochromism, such that red shifting of the dye main absorption peak leads to increased near-IR loss. For all three wavelengths, dα/d*C* was found to decrease with inhomogeneous width Γ_s (as expected on the basis of the previously described Γ_s−ν_{max} trends) for the 4E6m/Bisphenol A polycarbonate series, indicating that broadening is not responsible for the experimentally determined near-IR loss behavior in these systems. Thus, as the main peak is red shifted, even while being narrowed, a greater portion of the red absorption tail is deposited into the near-IR region, raising the baseline between the overtone peaks.

Because this is a strongly dipole-unallowed energy region for transitions (gap state region) where absorption is extremely weak, very small changes in main peak position that transfer the red tail to lower energies have large effects on the total absorption, as seen experimentally. Further, as proposed earlier in the discussion, a tradeoff between the molecular hyperpolarizability β and the near-IR loss is expected on the basis of the observed dα/d*C*−ν_{max} behavior, because loss is reduced by smaller solvent shifts, whereas β is expected to improve with red shifting for a bathochromic system. Note, however, that this tradeoff must be examined carefully within the framework of the BLA and SCRF reaction scales, to ensure that the system is within the positive solvatochromism regime, and β is not decreasing with polarity.

ν_{max} vs Solvent Polarity Analyses. On the basis of the observation of solvatochromism-controlled near-IR loss for the 4E6m/polycarbonate family of materials, following Onsager continuum dielectric behavior,[72] it follows that a complete accounting of physical properties of the dye and polymer host materials responsible for near-IR loss requires a detailed analysis of the polarity of the polymer medium, which can be expressed in terms of its dielectric properties, i.e., refractive index *n* and dielectric constant ϵ. As discussed earlier, the analyses by Marder et al. and Marks et al. show that the polarity of the polymer matrix as well as the dye geometry, substituents, and dipole properties, can influence both the strength of the solvatochromic shift and the nonlinear optical activity.

Numerous dielectric models related to solvent polarity and solute dipole properties have been proposed[73−78] to account for the solvent shift, usually described by a quantity *F* referred to variously as polarity parameter[79] or solvent parameter,[80] modified by terms containing solute dipole moments and geometry, and which neglect short-range hydrogen bonding and other

specific interactions. Many of these functional forms can be shown to be special cases of a very generalized expression developed by Kawski:[73]

$$\Delta\nu_{max} = -\frac{m_A}{(1-\alpha_0 f')}\left(\frac{f}{1-\alpha_0 f} - \frac{f'}{1-\alpha_0 f'}\right) - \frac{\mu_e^2 - \mu_g^2}{2hc}\frac{(2-\alpha_0 f')f'}{(2-\alpha_0 f')^2} \quad (16)$$

where

$$m_A = \mu_g(\mu_e - \mu_g)/hc \quad (16a)$$

μ_e and μ_g are solute permanent ground and excited state dipole moments, respectively, α_0 is the linear polarizability of the solute, f and f' are referred as reaction field factors related to the solvent dielectric properties (n and ϵ, defined for eq 11), and the solute shape and cavity radius:

$$f = \frac{2}{abc}\frac{\epsilon - 1}{2\epsilon + 1}F(\epsilon, A_s) \qquad f' = \frac{2}{abc}\frac{n^2 - 1}{2n^2 + 1}F(n^2, A_s) \quad (16b)$$

where $2a$, $2b$, and $2c$ are the major and two minor axes of an ellipsoidal solute cavity;

$$F(\epsilon, A_s) = \frac{3A_s(1-A_s)(2\epsilon+1)}{2[\epsilon - (\epsilon-1)A_s]}$$

$$F(n^2, A_s) = \frac{3A_s(1-A_s)(2n^2+1)}{2[n^2 - (n^2-1)A_s]} \quad (16c)$$

and A_s is a solute shape factor given by

$$A_s = \frac{abc}{2}\int_0^\infty \frac{ds}{(s+a^2)^{3/2}(s+b^2)^{1/2}(s+c^2)^{1/2}} \quad (16d)$$

A_s increases as the width-to-length ratio of the ellipsoidal dye cavity increases. As an approximation, the field factors can be expressed

$$f = (2/a^3)\Phi \qquad f' = (2/a^3)\Phi' \quad (17)$$

where

$$\Phi = \frac{\epsilon - 1}{2\epsilon + 1}F(\epsilon, A_s) \qquad \Phi' = \frac{n^2 - 1}{2n^2 + 1}F(n^2, A_s) \quad (17a)$$

The generalized Kawski relation can be expressed more conveniently in terms of a function F_K that groups all terms in the general expression except $(\mu_e^2 - \mu_g^2)/2hc$ as

$$\nu_{max} = -mF_K + \nu_A^0 \quad (18)$$

where

$$m = (\mu_e^2 - \mu_g^2)/2hc \quad (18a)$$

and

$$F_K = \frac{2\mu_g\Delta\mu}{(\mu_e^2 - \mu_g^2)}\frac{1}{1-\alpha_0 f'}\left(\frac{f}{1-\alpha_0 f} - \frac{f'}{1-\alpha_0 f'}\right) + \frac{(2-\alpha_0 f')f'}{(2-\alpha_0 f')^2} \quad (18b)$$

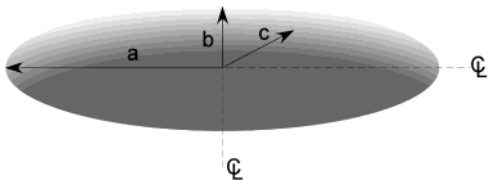

Figure 14. Geometry of 4E6m dye molecule in the framework of the Kawski dielectric model. (a) is along the ZINDO dipole axis; (b) and (c) are distance vectors from the molecular center at the dipole axis to spacer group endpoints. Shape factor A_s is determined from ratio a/c (given $b/c = 1$).

This form of the generalized Kawski relation allows for correlation of experimentally determined peak transition frequency ν_{max} with a solvent shift function F_K determined from the predicted dye molecular properties and polymer dielectric properties, with theoretical slope $m = (\mu_e^2 - \mu_g^2)/2hc$. The n and ϵ values for each of the polymer hosts of this study were predicted using the Accelrys, Inc. Cerius[2] SYNTHIA quantitative structure−property relationship (QSPR) model developed by Bicerano.[81] This model is based strictly on the topology of the polymer structure, i.e., connectivity indices derived from non-hydrogen-bonded graph theory, based entirely on the atoms and bonds, without the need for correlation with group contributions.

The 4E6m chromophore molecule was modeled using the Accelrys, Inc. Cerius[2] COMPASS open force-field method to geometrically minimize the structure, and a semiempirical method, Accelrys, Inc. Cerius[2] ZINDO, to calculate the configuration interaction (CI) single-point energies for ground and excited state conformations, from which the frequency-dependent transition dipoles, ground and excited state permanent dipole moments (μ_g and μ_e), and linear polarizability (α_0) were computed, along with the cavity radius (a_0) in a polycarbonate dielectric medium applying a self-consistent reaction-field, and the unperturbed $\pi \rightarrow \pi^*$ transition frequency in a vacuum (ν_A^0). For this calculation, the intermediate neglect of differential overlap version 1 (INDO/1) Hamiltonian was chosen, and the Tamm−Danncoff approximation (TDA) was selected for computation of the linear polarizability α_0. The ZINDO-derived values of μ_g and μ_e were 17.03 and 23.42 D, respectively, giving a difference between excited and ground dipole moments $\Delta\mu$ of 6.39 D; the TDA-derived α_0 was computed as 41.12 Å^3, and ν_A^0 was computed as 2.61 eV (21 041 cm^{-1}).

Highly linear correlations were found with the Kawski solvent polarity relation for the 4E6m doped polycarbonate series, in all cases involving the predicted material parameters with and without simplifications involving the dye geometry and polarizability. However, the agreement of the experimental slope with the theoretical slope, based on the ZINDO predicted dipole moments, required careful definition of the dye ellipsoidal shape factor and cavity radius. A detailed analysis revealed that the generalized Kawski relation closely approaches the theoretical slope when $2a$ is defined as the length of the ZINDO dipole axis (21.28 Å), b and c are distance vectors from the molecular center at the dipole axis to the dialkyl spacer group endpoints ($b = c = 5.484$ Å; see Figure 14), and the parameter a is defined as the Onsager cavity radius, a_0, with the approximation set forth by Kawski[73] as

$$a_0 = (2\alpha_0)^{1/3} \ (=4.35 \text{ Å}) \quad (19)$$

The resulting shape factor A_s for this geometry is 0.18. The experimental peak transition frequencies are plotted against the Kawski relation (F_K) incorporating these geometric definitions

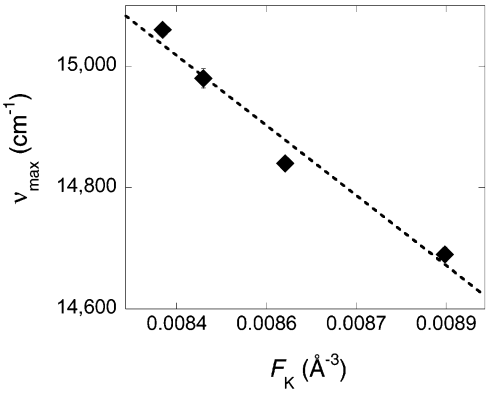

Figure 15. Main peak position ν_{max} for 4E6m/Bisphenol A polycarbonate series of guest−host materials at a dye concentration of 205 μmol/g of polymer, plotted as a function of the generalized Kawski dielectric relation with SYNTHIA-predicted polymer dielectric properties (n and ϵ), ZINDO-predicted 4E6m dye dipole moments (μ_e and μ_g) and linear polarizability (α), and shape factor (A_s) based on the geometry of Figure 14.

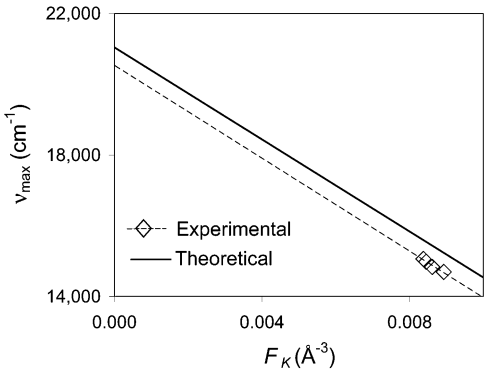

Figure 16. Experimental vs theoretical peak position ν_{max} for 4E6m/Bisphenol A polycarbonate series of guest−host materials at a dye concentration of 205 μmol/g of polymer, plotted against the generalized Kawski dielectric relation for SYNTHIA-predicted polymer dielectric properties (n and ϵ) and ZINDO-predicted 4E6m dye dipole moments (μ_e and μ_g), linear polarizability (α), shape factor (A_s), with spherical cavity radius (a_0) calculated using Kawski's approximation ($a_0 = (2\alpha)^{1/3}$), extrapolated to the vacuum level transition frequency ν_A^0.

in Figure 15, showing good linear correlation ($R^2 = 0.97$) with a slope m for the 4E6m/polycarbonates corresponding to a difference between ground and excited state dipole moments $\Delta\mu$ of 6.45 D in conjunction with the ZINDO-predicted μ_g, in very close agreement with the ZINDO $\Delta\mu$ value of 6.39 D. The experimental data are extrapolated to the vacuum transition frequency ν_A^0 and compared against the theoretical correlation (based on the SYNTHIA- and ZINDO-predicted parameters) in Figure 16. This comparison shows reasonable agreement between experimentally and theoretically derived ν_A^0's. A summary of molecular parameters used and results of the Kawski solvent shift model are given in Table 1.

Most of the various solvent shift relationships published in the literature correspond to simplifications of the generalized Kawski relation (eqs 16−18) based on assumptions such as equivalence of emission and absorption band shifts, specific solute cavity geometry, and relationship between solute cavity radius and linear polarizability. McRae[75] pointed out earlier that unless the solvent and solute are both polar, solvatochromic shifts in corresponding emission and absorption bands are predicted to be equal. A form of the Chamma−Viallet−Kawski (CVK) relation is arrived at with this assumption and the Kawski cavity approximation $2\alpha_0/a_0^3 = 1$ (valid for a wide range of

TABLE 1: Summary of Kawski Dielectric Function Parameters

dye Onsager cavity radius, a_0 (Å)	4.35
cavity radius basis	$a_0 = (2\alpha)^{1/3}$ (a)
ellipsoid axial shape dimension, a (Å)	10.64
ellipsoid radial shape dimensions, b and c (Å)	5.48
dye polarizability, α (Å^3)	41.12[(b)]
experimental slope-derived $\Delta\mu$ (D)	6.45
theoretical (ZINDO) $\Delta\mu$ (D)	6.39
ν_A^0(theoretical) − ν_A^0(experimental) (cm^{-1})	540
correlation coefficient (R^2)	0.97

[a] Kawski cavity radius approximation. [b] ZINDO-calculated polarizability with Tamm−Dancoff Approximation (TDA).

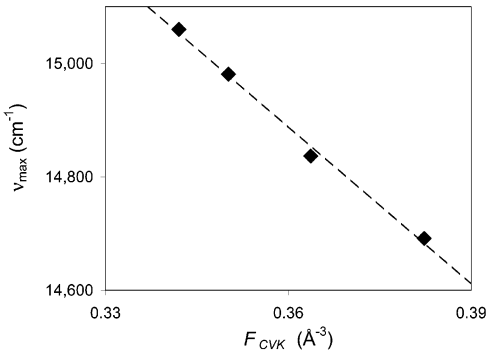

Figure 17. Main peak position ν_{max} for 4E6m/Bisphenol A polycarbonate series of guest−host materials at a dye concentration of 205 μmol dye per gram of polymer, plotted as a function of the Chamma−Viallet−Kawski dielectric relation with SYNTHIA-predicted polymer dielectric properties (n and ϵ).

systems), and assuming a spherical cavity ($a = b = c$, $A_s = {}^1/_3$ and $F(\epsilon,A_s) = F(n^2,A_s) = 1$):[73,74]

$$\nu_{max} \cong -2\frac{(\mu_e^2 - \mu_g^2)}{hca_0^3}F_{CVK} + \nu_A^0 \qquad (20)$$

where

$$F_{CVK} = \frac{2n^2+1}{2(n^2+2)}\left(\frac{\epsilon-1}{\epsilon+2} - \frac{n^2-1}{n^2+2}\right) + \frac{3}{2}\frac{n^4-1}{(n^2+2)^2} \qquad (20a)$$

The experimental peak transition frequencies are plotted directly against F_{CVK} in Figure 17, showing exceptional linear correlation ($R^2 = 0.995$). With the dye cavity radius approximation as given by Kawski (4.35 Å), the experimental slope of the CVK correlation leads to a values for $\Delta\mu$ (given the ZINDO-predicted μ_g) and extrapolated vacuum transition frequency ν_A^0 in poor agreement with the ZINDO calculated values. Notwithstanding this lower accuracy in predicting the dye $\Delta\mu$ and ν_A^0 parameters and less general applicability expected across structural families, relative to the generalized Kawski model, the CVK model is the least computationally complex among those explored and requires no prior knowledge of the dye ground and excited state dipole moments, polarizability, or shape factor. As such, it is the most practical among the polarity models investigated for predicting peak shift behavior within a given polymer structural class. If the McRae approximation of equal emission and absorption solvent shifts in polycarbonates can be demonstrated by further investigation, the Chamma−Viallet−Kawski model may have more broad applicability.

In addition to the generalized Kawski and the Chamma−Viallet−Kawski relations, alternative solvent polarity relations (with solvent shift functions F and slopes m) were evaluated for correlation with the experimental peak transition frequencies

ν_{max}, each of which are special cases of the generalized Kawski relation (eqs 16−18). Four of these use the same simplifying assumptions as invoked by the Chamma−Viallet−Kawski model (except for equivalence of emission and absorption band shifts):

McRae relation[75]

$$F_M = \frac{n^2-1}{2n^2+1} + \frac{2\mu_g\Delta\mu_g}{(\mu_e^2-\mu_g^2)}\left(\frac{\epsilon-1}{\epsilon+2} - \frac{n^2-1}{n^2+2}\right)$$

$$\text{slope } m_M = -\frac{(\mu_e^2-\mu_g^2)}{hca_0^3} \quad (21a)$$

Bakhshiev relation[77]

$$F_B = \frac{2n^2+1}{n^2+2}\left(\frac{\epsilon-1}{\epsilon+2} - \frac{n^2-1}{n^2+2} + \frac{(\mu_e^2-\mu_g^2)}{2\mu_g\Delta\mu}\frac{n^2-1}{n^2+2}\right)$$

$$m_B = -\frac{2\mu_g\Delta\mu}{hca_0^3} \quad (21b)$$

Liptay relation[82]

$$F_L = \frac{\epsilon-1}{\epsilon+2} - \frac{(\mu_e^2-\mu_g^2)}{2\mu_g\Delta\mu}\frac{n^2-1}{n^2+2}z \qquad m_L = -\frac{2\mu_g\Delta\mu}{hca_0^3} \quad (21c)$$

Ooshika relation[78]

$$F_O = \frac{2(\epsilon-1)}{2\epsilon+1} + \frac{\Delta\mu}{\mu_g}\frac{n^2-1}{2n^2+1} \qquad m_O = -\frac{\mu_g\Delta\mu}{hca_0^3} \quad (21d)$$

Two more general solvent polarity relations explored were expanded Bakhshiev relation[76]

$$F_{Be} = \left(\frac{2n^2+1}{n^2+2}\right)^2\left(\frac{\epsilon-1}{\epsilon+2} - \frac{n^2-1}{n^2+2} + \frac{(\mu_e^2-\mu_g^2)}{2\mu_g\Delta\mu}\frac{n^2-1}{n^2+2}\right) + (3380\text{ cm}^{-1})\frac{hca_0^3}{2\mu_g\Delta\mu} \qquad m_{Be} = -\frac{2\mu_g\Delta\mu}{hca_0^3} \quad (21e)$$

generalized Liptay relation[82]

$$F_{Lg} = \frac{(n^2+g_0)(\epsilon-1)-(\epsilon+g_0)(n^2-1)}{[(1-h_0)\epsilon+(g_0+h_0)][(1-h_0)n^2+(g_0+h_0)]} - \frac{\mu_e^2-\mu_g^2}{(\Delta\mu)^2}\frac{\epsilon-1}{(1-h_0)\epsilon+(g_0+h_0)} \quad (21f)$$

$$g_0 = \frac{A_s}{1-A_s} \qquad h_0 = \frac{3\alpha_0 A_s}{a^3} \qquad m_{Lg} = \frac{3}{2}\frac{(\Delta\mu)^2}{hca^3} \quad (21f\text{-}1)$$

For all of these solvent shift relations except the McRae relation ($R^2 = 0.73$), a strong linear dependence of the experimental peak transition frequency ν_{max} with the parameter F was observed ($R^2 = 0.96-0.998$), providing a high level of confidence in the SYNTHIA-predicted values of the polymer dielectric properties and in the earlier assertion that the observed peak shifts for 4E6m in the Bisphenol A polycarbonate class of polymers are due to positive solvatochromism. Of all the polarity functions investigated, the best linear fits were shown for the Chamma−Viallet−Kawski relation ($R^2 = 0.995$), and the expanded ($R^2 = 0.998$) and simplified ($R^2 = 0.99$) Bakhshiev relations. None of these simplified relations provided slope-derived values of $\Delta\mu$ in agreement with the ZINDO-derived values when the Kawski approximated cavity radius was utilized. Note the demonstrated ν_{max}−polarity behavior described here is entirely consistent with the ν_{max}−solubility behavior shown earlier in the discussion, in that the highly dipolar dye 4E6m is expected to experience greater solubility (lower heats of mixing) in polymers exhibiting higher polarity (as indeed has been shown by the SYNTHIA model predictions). Moreover, for a solvent−solute system response consistent with a classical continuum dielectric reaction field, the solvent reorganization energy is lowered so that formation of an oriented solvent cage around the solute stabilizes the excited state. The increased solubility of the dye provides for greater dispersions and polar interactions (inductions), which both Marcus[66] and Matyushov and Schmid[61] showed contribute to the solvent shift. This solvatochromic behavior is also expected to closely follow the response of the hyperpolarizability to a solvent reaction field described by Marks et al.[14] for a chromophore closer to structure (I) in Figure 7 on the BLA scale, in that an increase in solvent polarity gives rise to higher β.

The generalized Kawski dielectric model (eqs 16−18) appears to provide the most accurate representation of the observed solvatochromic shift behavior by the polycarbonates, based on the combination of slope-derived change in dipole moment on excitation and intercept-derived vacuum-level transition frequency, compared with ZINDO calculated values. On the basis of the accuracy of this model, it would appear that the Onsager spherical cavity radius predicted by the Kawski approximation, i.e., $\alpha_0/a_0^3 = 1/2$ (with α_0 based on the Tamm-Dancoff Approximation), is appropriate and internally consistent with the generalized Kawski model. The accuracy and self-consistency of this dielectric model is felt to be due in large part to its accounting for the ellipsoidal geometry of the dye molecule, which is not accounted for by the other well-correlated models.

The Liptay (eq 21f) and Bakhshiev models (eqs 21b and 21c) represent intermediate levels of complexity and input material property parameters but may be generally applicable to NLO dyes in polycarbonates of various structures.

Loss−Concentration Slope dα/dC vs Polarity Function F Relations. The experimentally determined near-IR loss vs concentration slopes dα/dC are plotted against the solvent polarity parameter F for the generalized Kawski relation (eqs 16−18), at wavelengths of 1060, 1300, and 1550 nm, in Figure 18a−c. As expected from the linear dependence of dα/dC on peak frequency in conjunction with the linear dependence of peak frequency with the solvent polarity functions, strong linear correlations of dα/dC with solvent polarity are seen for the Kawski solvent shift model at all three wavelengths. Similar correlations were found for the other well-correlated solvent shift models. These correlations for dα/dC vs F provide the basis for a predictive model of near-IR loss for dye-doped polycarbonate, through the polymer dielectric properties n and ϵ in the parameter F.

For the range of n, ϵ, μ_g, and μ_e values explored, our analysis shows that for the generalized Kawski model, the $\nu_{max}-F_K$ slope is minimized for increasing values of the shape factor A_s, indicating that the solvent shift $\Delta\nu_{max}$, and hence near-IR loss, is minimized by an increased chromophore width-to-length ratio for 4E6m-like dyes in polycarbonates. For a given shape factor, decreasing the value of the ellipsoidal axis parameter a was seen to decrease the slope rapidly. These parametric trends for A_s and a point toward reducing near-IR loss by using a shorter, more spherically shaped dye. However, because changes in dye

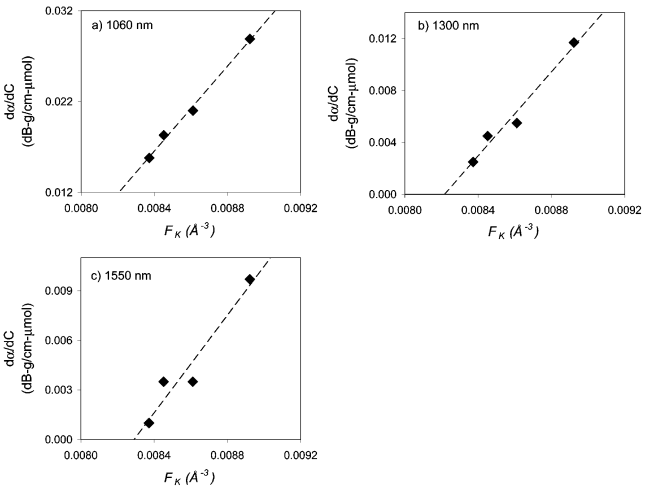

Figure 18. Measured PDS absorption loss−concentration slope vs generalized Kawski dielectric solvent shift function calculated from predicted polymer n and ϵ and predicted dye dipole moments μ_g and μ_e and static polarizability α_0 at wavelengths of (a) 1060 nm, (b) 1300 nm, and (c) 1550 nm.

structure were not included in this investigation, a separate study that systematically varies the dye geometry is required to test the above analyses regarding dye size and shape. Further, the dye 4E6m used in this study has a relatively large ellipsoidal aspect ratio, given the short dialkyl spacer length compared with FTC and LMCO-46m. As such, the solvatochromism and broadening observed for 4E6m-doped polycarbonates may represent one end of a spectrum of dye−polymer interaction behavior, so that a physical upper limit for solvatochromism-controlled near-IR loss exists as the dye width-to-length ratio increases.

Conclusions

The concentration dependence of optical absorption spectral behavior was investigated by photothermal deflection spectroscopy for glassy, amorphous nonlinear optical dye−polymer guest−host materials based on the nonlinear optical dye 4E6m, a structural analogue of the well-known nonlinear optical dye FTC, incorporated into a series of aromatic polymers composed of Bisphenol A polycarbonates. Linear or approximately linear dependence of absorption loss vs dye concentration at three spectral minima (1060, 1300, and 1550 nm) was observed for all guest−host materials in the series reported here, indicating a lack of specific or strong-binding interactions between the dye and polymer. Determination of the loss−concentration slope behavior at each spectral minimum, in conjunction with red shifting behavior of the main absorption peak, is shown to be a valuable approach for revealing structure−property relationships based on variations in polymer dielectric properties. Knowledge and minimization of the polymer host near-IR optical loss is not sufficient for the understanding and control of loss for dye-doped polymers.

The loss−concentration slope behavior at a spectral minimum of 1060 nm was found to reflect the solvatochromic shift behavior of the main absorption peak for all polymers studied and can be ascribed to the close proximity of this spectral feature to the position of the absorption maximum, such that more red shifted absorption shows higher loss at 1060 nm. At spectral minima of 1300 and 1550 nm, the loss−concentration slope variation with the position of the main absorption peak (ν_{max}, cm^{-1}) exhibited increasing loss−concentration slope at 1300 and 1550 nm as ν_{max} decreased, indicating near-IR loss behavior completely dominated by solvatochromism, wherein the more red shifted the main absorption peak is, the higher the near-IR loss. This behavior is despite the decreased inhomogeneous broadening associated with red shifting, suggesting that the narrowing with decreasing dye electronic transition energy is insufficient to overcome transfer of a large component of the absorption distribution into the near-IR, with increasing polymer polarity, for these polycarbonate-based guest−host systems. This bathochromic shift behavior, and the corresponding loss−concentration slope behavior, are well correlated to the predicted dielectric properties of the polymer, as described by a variety of solvent polarity models. Of these solvent polarity models, the generalized Kawski relation most accurately and self-consistently reproduced the induced change in dipole moment predicted by the semiempirical ZINDO model and incorporates dye geometric shape effects. The near-IR loss behavior is shown to be well correlated with these solvent shift models, suggesting the fundamental material absorption in the near-IR may be predicted on the basis of the polymer dielectric properties (index of refraction and dielectric constant). The system 4E6m/Red Cross polycarbonate is projected to exhibit low loss (<1 dB/cm) at 1550 nm for loading levels necessary for a practical device (500 μmol of dye/g of polymer, 25 wt %).

These results show that the excited state of the dye electronic transition is stabilized by a more polar dielectric medium and are consistent with the Onsager dielectric continuum model. The observed increase in near-IR loss with red shifting as polymer polarity increases is at odds with expected improvements in the molecular nonlinearity β under the same conditions. This suggests a tradeoff between these two behaviors, such that an optimum combination of polymer dielectric properties, dye geometry, and dipole moments exists for a maximized device gain product. The correlation of these properties with the generalized Kawski solvent polarity relation shows that a shorter and more spherically symmetric dye shape may lead to reduced near-IR loss, but this interpretation needs to be confirmed by further experimental investigation of dye geometry in guest−host materials.

Acknowledgment. R.B. gratefully acknowledges Lockheed Martin Corp. for financial support through the Lockheed Martin-Stanford Honors Co-op Program and independent research and development funding. R. Barto acknowledges William W. Anderson, Lawrence J. Dries, Dexter G. Girton, and Wendell D. Eades from Lockheed Martin, Andrew J. Skumanich from Applied Materials, Carlton H. Seager from Sandia National Laboratories, and Simon McGrother and Klaus Stark from Accelrys, Inc. for significant technical guidance and many helpful discussions. Finally, we express sincere gratitude to James Cella and Chris Kapusta of General Electric Corp. for providing Red Cross and Bisphenol A-*co*-fluorenone polycarbonates for this study.

References and Notes

(1) Senior, J. M. *Optical Fiber Communications, Principles and Practice*; Prentice Hall: New York, 1992.

(2) Ackerman, E. I.; Cox, C. H., III. *IEEE Microwave Magn.* **2001**, *2*, 50.

(3) Hasanein, A. A. In *Modern Nonlinear Optics*; Kielich, S., Ed.; Advances in Chemical Physics LXXXV; John Wiley & Sons: New York, 1993; Part 2.

(4) Dagli, N. *IEEE Trans. Microwave Theor. Techn.* **1999**, *47*, 1151.

(5) Dalton, L. R.; Harper, A. W.; Chen, J.; Sun, S.; Mao, S.; Garner, S.; Chen, A.; Steier, W. H. *Crit. Rev. Opt. Sci. Technol.* **1997**, *CR68*, 313.

(6) Dalton, L. R.; Harper, A. W.; Robinson, B. H. *Proc. Nat. Acad. Sci. U.S.A.* **1997**, *94*, 4842.

(7) Robinson, B. H.; Dalton, L. R.; Harper, A. W.; Ren, A.; Wang, F.; Zhang, C.; Todorova, G.; Lee, M.; Aniszfeld, R.; Garner, S.; Chen, A.; Steier, W. H.; Houbrecht, S.; Persoons, A.; Ledoux, I.; Zyss, J.; Jen, A. K. Y. *Chem. Phys.* **1999**, *245*, 35.

(8) Harper, A. W.; Wang, F.; Chen, J.; Lee, M.; Dalton, L. R. *ACS Symp. Ser.* **1999**, *726*, 160.

(9) Robinson, B. H.; Dalton, L. R. *J. Phys. Chem. A* **2000**, *104*, 4785.

(10) Jen, A. K. Y.; Luo, J.; Ma, H.; Haller, M.; Barto, R. R.; Frank, C. W. *Proc. SPIE* **2002**, *4809*, 79.

(11) Wu, X.; Jen, A. K. Y. *Mater. Res. Soc. Symp. Proc.* **2000**, *598*, BB11.45/1.

(12) Zheng, L.; Sassa, T.; Jen, A. K. Y. *Mater. Res. Soc. Symp. Proc.* **2002**, *725*, 219.

(13) Li, D.; Marks, T. J.; Zhang, C.; Yang, J.; Wong, G. K. *Proc. SPIE* **1990**, *1337*, 341.

(14) Albert, I. D. L.; Marks, T. J.; Ratner, M. A. *J. Phys. Chem.* **1996**, *100*, 9714.

(15) Ma, H.; Jen, A. K. Y.; Wu, J.; Wu, X.; Liu, S.; Shu, C.-F.; Dalton, L. R.; Marder, S. R.; Thayumanavan, S. *Chem. Mater.* **1999**, *11*, 2218.

(16) Wang, F.; Harper, A. W.; Lee, M. S.; Dalton, L. R.; Zhang, H.; Chen, A.; Steier, W. H.; Marder, S. R. *Chem. Mater.* **1999**, *11*, 2285.

(17) Marder, S. R.; Kippelen, B.; Jen, A. K. Y.; Peyghammbarian, N. *Nature* **1997**, *388*, 845.

(18) Marder, S. R.; Gorman, C. B.; Meyers, F.; Perry, J. W.; Bourhill, G.; Bredas, J.-L.; Pierce, B. M. *Science* **1994**, *265*, 632.

(19) Jacques, P. *J. Phys. Chem.* **1986**, *90*, 5535.

(20) Barto, R. R.; Frank, C. W.; Bedworth, P. V.; Epstein, J.; Ermer, S. P.; Taylor, R. E. *Proc. SPIE* **2003**, *4991*, 575.

(21) Ermer, S.; Lovejoy, S. M.; Bedworth, P. V.; Leung, D. S.; Warren, H. B.; Epstein, J. A.; Girton, D. G.; Dries, L. S.; Taylor, R. E.; Barto, R. R., Jr.; Eades, W.; Van Eck, T. E.; Moss, A. S.; Anderson, W. W. *Adv. Funct. Mater.* **2002**, *12*, 605.

(22) Ermer, S.; Barto, R. R., Jr.; Taylor, R. E.; Bedworth, P. V.; Epstein, J. *Polym. Mater. Sci. Eng.* **2003**, *88*, 126.

(23) Ma, H.; Liu, S.; Luo, J.; Suresh, S.; Liu, L.; Kang, S. H.; Haller, M.; Sassa, T.; Dalton, L. R.; Jen, A. K. Y. *Adv. Funct. Mater.* **2002**, *12*, 565.

(24) Dureiko, R. D.; Schuele, D. E.; Singer, K. D. *J. Opt. Soc. Am. B* **1998**, *15*, 338.

(25) Barto, R. Unpublished experimental observations, 2000.

(26) Ermer, S. P.; Girton, D. G.; Dries, L. J.; Taylor, R. E.; Eades, W. D.; VanEck, T. E.; Moss, A. S.; Anderson, W. W. *Proc. SPIE* **2000**, *3949*, 148.

(27) Wang, F.; Ren, A. A.; He, M.; Lee, M. S.; Harper, A. W.; Dalton, L. R.; Zhang, H.; Garner, S. M.; Chen, A.; Steier, W. H. *Polym. Prepr. (Am. Chem. Soc., Div. Polym. Chem.)* **1998**, *39*, 1065.

(28) Ahn, S.-W.; Steier, W. H.; Kuo, Y.-H.; Oh, M.-C.; Lee, H.-J.; Zhang, C.; Fetterman, H. R. *Opt. Lett.* **2002**, *27*, 2109.

(29) Oh, M.-C.; Zhang, H.; Zhang, C.; Erlig, H.; Chang, Y.; Tsap, B.; Chang, D.; Szep, A.; Steier, W. H.; Fetterman, H. R.; Dalton, L. R. *IEEE J. Sel. Top. Quantum Elect.* **2001**, *7*, 826.

(30) Zhang, C.; Dalton, L. R.; Oh, M.-C.; Zhang, H.; Steier, W. H. *Chem. Mater.* **2001**, *13*, 3043.

(31) Zhang, H.; Oh, M.-C.; Szep, A.; Steier, W. H.; Zhang, C.; Dalton, L. R.; Erlig, H.; Chang, Y.; Chang, D. H.; Fetterman, H. R. *Appl. Phys. Lett.* **2001**, *78*, 3136.

(32) Dalton, L. R.; Robinson, B. H.; Jen, A. K. Y.; Steier, W. H.; Nielsen, R. *Opt. Mater.* **2003**, *21*, 19.

(33) Luo, J.; Ma, H.; Haller, M.; Jen, A. K. Y.; Barto, R. R. *Chem. Commun.* **2002**, 888.

(34) Tanaka, K.; Gotoh, T.; Yoshida, N.; Nonomura, S. *J. Appl. Phys.* **2002**, *91*, 125.

(35) Jackson, W. B.; Amer, N. M. *AIP Conf. Proc.* **1981**, *73*, 263.

(36) Bennett, H. S.; Forman, R. R. *J. Appl. Phys.* **1977**, *48*, 432.

(37) Jackson, W. B.; Amer, N. M.; Boccara, A. C.; Fournier, D. *Appl. Opt.* **1981**, *20*, 1333.

(38) Rosencwaig, A.; Gersho, A. *J. Appl. Phys.* **1976**, *47*, 64.

(39) Boccara, A. C.; Fournier, D.; Badoz, J. *Appl. Phys. Lett.* **1980**, *36*, 130.

(40) Pitois, C.; Hult, A.; Wiesmann, D. *J. Opt. Soc. Am. B* **2001**, *18*, 908.

(41) Leovich, M.; Yaney, P. P.; Zhang, C. H.; Steier, W. H.; Oh, M.-C.; Fetterman, H. R.; Jen, A. K. Y.; Dalton, L. R.; Grote, J. G.; Nelson, R. L.; Zetts, J. S.; Hopkins, F. K. *Proc. SPIE* **2002**, *4652*, 97.

(42) Grote, J. G.; Zetts, J. S.; Nelson, R. L.; Diggs, D. E.; Hopkins, F. K.; Yaney, P. P.; Zhang, C.; Steier, W. H.; Oh, M.-C.; Fetterman, H. R.; Jen, A. K. Y.; Dalton, L. R.; Taylor, E. W.; Winter, J. E.; Sanchez, A. D.; Craig, D. M. *Proc. SPIE* **2002**, *4823*, 6.

(43) Kang, S. H.; Luo, J.; Ma, H.; Barto, R. R.; Frank, C. W.; Dalton, L. R.; Jen, A. K. Y. *Macromolecules* **2003**, *36*, 4355.

(44) Le Duff, A.-C.; Ricci, V.; Pliska, T.; Canva, M.; Stegeman, G. I.; Chan, K. P.; Twieg, R. *Appl. Opt.* **2000**, *39*, 947.

(45) Myers, A. B. *Annu. Rev. Phys. Chem.* **1998**, *49*, 267.

(46) Bondar, M. V.; Przhonskaya, O. V.; Tikhonov, E. A. *J. Phys. Chem.* **1992**, *96*, 10831.

(47) Finzi, L.; Zucchelli, G.; Garlaschi, F. M.; Jennings, R. C. *Biochemistry* **1999**, *38*, 10627.

(48) Kjaer, A. M.; Ulstrup, J. *J. Am. Chem. Soc.* **1988**, *110*, 3874.

(49) Kador, L. *J. Chem. Phys.* **1991**, *95*, 5574.

(50) Skinner, J. L.; Moerner, W. E. *J. Phys. Chem.* **1996**, *100*, 13251.

(51) Loring, R. F. *J. Phys. Chem.* **1990**, *94*, 513.

(52) Meskers, S. C. J.; Janssen, R. A. J.; Haverkort, J. E. M.; Wolter, J. H. *Chem. Phys.* **2000**, *260*, 415.

(53) Liebsch, A.; González, P. V. *Phys. Rev. B* **1984**, *29*, 6907.

(54) Kador, L.; Horne, D. E.; Moerner, W. E. *J. Phys. Chem.* **1990**, *94*, 1237.

(55) Moran, A. M.; Egolf, D. S.; Blanchard-Desce, M.; Kelley, A. M. *J. Chem. Phys.* **2002**, *116*, 2542.

(56) Obata, M.; Machida, S.; Horie, K. *J. Polym. Sci. B* **1999**, *37*, 2173.

(57) Dimroth, K.; Reichardt, C.; Siepmann, T.; Bohlmann, F. *Liebigs Ann. Chem.* **1963**, *661*, 1.

(58) Reichardt, C. *Solvents and Solvent Effects in Organic Chemistry*, 2nd ed.; VCH Publishers: Weinheim, Germany, 1988.

(59) Marcus, R. A. *J. Chem. Phys.* **1965**, *43*, 1261.

(60) Lacroix, P. L.; Malfant, I.; Iftime, G.; Razus, A. C.; Nakatani, K.; Delaire, J. A. *Chem. Eur. J.* **2000**, *6*, 2599.

(61) Matyushov, D. V.; Schmid, R. *J. Chem. Phys.* **1995**, *103*, 2034.

(62) Matyushov, D. V.; Schmid, R.; Ladanyi, B. M. *J. Phys. Chem. B* **1997**, *101*, 1035.

(63) Sevian, H. M.; Skinner, J. L. *J. Chem. Phys.* **1992**, *97*, 8.

(64) Singer, K. In *Polymers for Lightwave and Integrated Optics*; Hornak, L. A., Ed.; Marcel Dekker: New York, 1992.

(65) Karelson, M. M.; Zerner, M. C. *J. Phys. Chem.* **1992**, *96*, 6949.

(66) Marcus, R. A. *J. Chem. Phys.* **1965**, *43*, 1261.

(67) Barton, A. F. M. *Handbook of Solubility Parameters and Other Cohesion Parameters*; CRC Press: Boca Raton, FL, 1983.

(68) Hildebrand, J. H.; Scott, R. L. *The Solubility of Nonelectrolytes*; Reinhold: New York, 1949.

(69) Scatchard, G. *Chem. Rev.* **1931**, *8*, 321.

(70) Brandrup, J.; Immergut, E. H.; Grulke, E. A. *Polymer Handbook*; Wiley & Sons: New York, 1999.

(71) Sperling, L. H. *Introduction to Physical Polymer Science*; Wiley-Interscience: New York, 1992.

(72) Onsager, L. *J. Am. Chem. Soc.* **1936**, *58*, 1486.

(73) Kawski, A. *Z. Naturforsch. A* **2002**, *57*, 255.

(74) Chamma, A.; Viallet, P. *C. R. Acad. Sci., Ser. C* **1970**, *270*, 1901.

(75) McRae, E. G. *J. Phys. Chem.* **1957**, *61*, 562.

(76) Mirashi, L. S. P.; Varkhede, R. S. *Indian J. Phys. B* **1990**, *64*, 407.

(77) Bakhshiev, N. G. *Opt. Spectrosk.* **1964**, *16*, 446.

(78) Ooshika, Y. *J. Phys. Soc. Jpn.* **1954**, *9*, 594.

(79) Renge, I. *J. Phys. Chem. A* **2000**, *104*, 3869.

(80) Otsuki, S.; Taguchi, T. *Bull. Chem. Soc. Jpn.* **1996**, *69*, 2525.

(81) Bicerano, J. *Prediction of Polymer Properties*; Marcel Dekker: New York, 2002.

(82) Liptay, W. *Z. Naturforsch.* **1965**, *20a*, 1441.